Computed tomography and radiographic assessment of congruity between the ulnar trochlear notch and humeral trochlea in large breed dogs

Sofia Alves-Pimenta[1,2]; Mário M. Ginja[2,3]; Armando M. Fernandes[4]; António J. Ferreira[5]; Pedro Melo-Pinto[2,6]; Bruno Colaço[1,2]

[1]Department of Animal Science, School of Agrarian and Veterinary Sciences, University of Trás-os-Montes and Alto Douro, Vila Real, Portugal; [2]CITAB – Centre for the Research and Technology of Agro-Environmental and Biological Sciences, University of Trás-os-Montes and Alto Douro, Vila Real, Portugal; [3]Department of Veterinary Science, School of Agrarian and Veterinary Sciences, University of Trás-os-Montes and Alto Douro, Vila Real, Portugal; [4]INOV – INESC Inovação, Lisbon, Portugal; [5]Clinical Department, Faculty of Veterinary Medicine, University of Lisbon, Lisboa, Portugal; [6]Department of Engineering, University of Trás-os-Montes and Alto Douro, Vila Real, Portugal

Keywords
Elbow dysplasia, congruity, medial coronoid process, radiographic anatomy, computed tomography, canine, dog

Summary

Objective: Assess the fit between the ulnar trochlear notch (UTN) and humeral trochlea (HT) in elbow radiographs and computed tomography (CT) images by measuring the curvature radii in normal joints.

Methods: Mediolateral extended view (MLE) and CT were performed on 16 elbows from cadaveric dogs weighing over 20 kg. Curves were traced at the subchondral level from the UTN central ridge and the HT sagittal groove related to the UTN on ~132° joint extension. Curvature radii were achieved using appropriate computer software.

Results: Intraclass correlation coefficient between MLE/CT measurements were statistically significant, with lower limits of a 95% confidence interval (CI) >0.75. The mean differences between MLE/CT measurements were -0.71 mm (95% CI: -0.97 to -0.45) for UTN and -1.04 mm (95% CI: -1.21 to -0.87) for HT. The UTN and HT curvature radii typology were similar, with maximum radius values at the starting point and two intermediate peaks. The UTN curvature radii were bigger than the HT radii, with the largest differences in the most proximal aspect of the joint and in the second intermediate peak.

Clinical significance: To the authors' knowledge, this is the first report on humeroulnar congruity through curvature radii evaluation. The software and methodology proposed enabled an adequate UTN and HT radii curvature assessment in MLE and CT images. Comparative studies in normal and dysplastic dogs of various breeds could better clarify the role of UTN and HT curvature radii in elbow incongruity and dysplasia.

Correspondence to:
Dr. Sofia Alves-Pimenta, MVM
Department of Animal Science
Trás-os-Montes and Alto Douro University
5001–801 Vila Real
Portugal
Phone: +351 259 350 403
Fax: +351 259 350 480
E-mail: salves@utad.pt

ORCID iD:
SAP: http://orcid.org/0000-0001-9842-1759
MMG: http://orcid.org/0000-0002-0464-7771
AMF: http://orcid.org/0000-0001-7850-0847
AJF: http://orcid.org/0000-0002-0142-6578
PMP: http://orcid.org/0000-0001-8257-0143
BC: http://orcid.org/0000-0003-4879-8624

Vet Comp Orthop Traumatol 2017; 30: 8–14
https://doi.org/10.3415/VCOT-16-03-0045
Received: March 12, 2016
Accepted: September 27, 2016
Epub ahead of print: November 16, 2016

Financial Support:
This work is supported by: European Investment Funds by FEDER/COMPETE/POCI– Operational Competitiveness and Internationalization Program, under Project POCI-01–0145-FEDER-006958 and National Funds by FCT – Portuguese Foundation for Science and Technology, under the project UID/AGR/04033.

Introduction

Elbow dysplasia is a developmental disorder and a common cause of osteoarthritis and severe thoracic limb lameness in young large and giant breed dogs (1, 2). A method for early detection of joint changes would improve screening effectiveness and avoid the transmission of the disease genes to offspring (3).

Elbow incongruity plays an important role in the aetiology, treatment options and prognosis of elbow dysplasia (4, 5). Altered loading patterns result in increased stress on the elbow medial compartment (6–8). A limited degree of joint incongruity is considered physiological, but severe incongruity is deemed pathological and may result in differing grades of elbow dysplasia (9-11). Elbow incongruity can occur in association with radioulnar unequal growth, differing radius and ulna length, or be due to humeroulnar incongruity, as a result of the elliptical shape of the ulnar trochlear notch (UTN) with a lesser curvature radius than the humeral trochlea (HT) (12).

Although humeroulnar incongruity has been postulated to predispose to medial coronoid disease, a quantitative technique to assess this finding does not exist and the evaluation remains subjective in nature (12). Some methods described in the literature recommend measuring the joint space to quantify incongruity, but this evaluation was influenced by elbow flexion angle, pronation and supination (4, 6). Other authors proposed defining the UTN and HT by the smallest circle that could be described (13,

14). As both the UTN and the HT do not have an exact circular profile, the definition of the smallest circle is merely approximate and conditioned by the subjective appraisal of the examiner (13-15). Some findings in arthroscopic studies, such as changes in the appearance of the UTN cartilage, with incomplete cartilage covering and erosion, could also suggest humeroulnar incongruity, but quantification was considered challenging (5, 16).

Despite its variable sensitivity, radiography is still the first-choice imaging method for elbow dysplasia screening (1). However, quantification of elbow geometry is hampered by the proximity of different surfaces that make up the joint (12, 17, 18). The development of further techniques to standardize radiographic interpretation of morphological variation in the humeroulnar joint shape has been claimed (12, 13). Computed tomography (CT) has several advantages in elbow dysplasia diagnosis, such as the ability to interpret images in different reconstructed views without the superimposition of osseous structures (9). New software functions offered by digital imaging also enable easier evaluation of joint images. Combining those diagnostic tools available in clinical practice with studies in elbow joint anatomy, may be useful to clarify elbow dysplasia development and enable the emergence of new therapeutic approaches (18).

The aim of the work presented here was to assess humeroulnar geometry and congruity, through the evaluation of the curvature radii from the central ridge of the UTN and the HT at the level of the sagittal groove, in radiographic and CT images of normal elbows. Software previously created and validated by the authors to measure the UTN and the HT radii of curvature was used (19, 20).

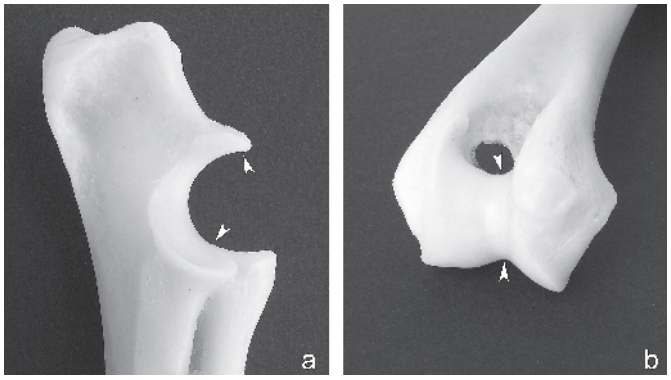

Figure 1 **a)** Medial view of the ulnar trochlear notch. The central ridge was assessed from the anconeal process to the base of the medial coronoid process (arrowheads). **b)** Caudal view of the humeral trochlear groove. The curvature was assessed in the sagittal plane from the most proximal and caudal point of the groove in contact with the central ulnar trochlear notch ridge, on ~132° elbow extension (arrowheads).

Materials and Methods

Animals included

Sixteen normal elbow joints from nine middle to large breed adult canine cadavers (from 1 to 12 years; 7.7 ± 4.3 years) weighing 20 to 46 Kg (32.2 ± 7.7 Kg) (six males and three females) were included. Two joints were excluded due to signs of slight elbow dysplasia in the radiographic examination, CT images, or both. The dogs had died for medical reasons unrelated to the study. All the animal procedures undertaken as part of the work described in this paper were carried out in compliance with the regulations of our institutions, and in accordance with the Portuguese and European regulations for animal use and care (European Directive 2010/63/EU and National Decree-Law 113/2013).

Image acquisition

First, a mediolateral extended radiographic view (MLE) was performed on every joint, using a computed x-ray device (13, 20). After that, the forelimbs were separated from the trunk by removing the extrinsic musculature of the forelimb from the scapula, and a complete transverse CT scan of each elbow was performed. Acquisition of CT data was performed on a multislice

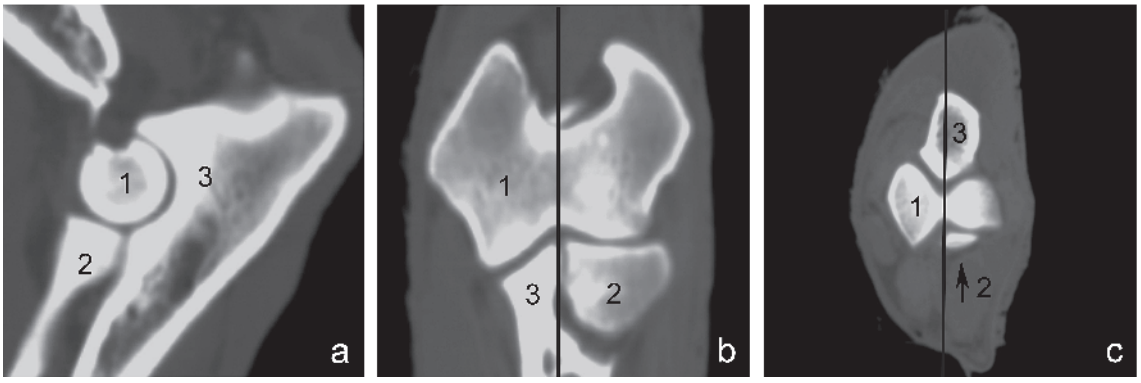

Figure 2 Computed tomography elbow slice and reconstructions. **a)** Sagittal; **b)** dorsal; and **c)** transverse views. The sagittal elbow plane used to study humeroulnar congruity was selected using computer software to cross a line (black line) that passed in the humeral trochlea groove in the dorsal and transverse elbow planes. 1 = humerus; 2 = radius; 3 = ulna.

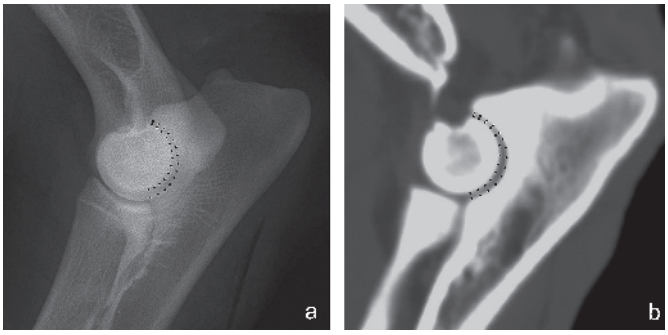

Figure 3 **a)** Mediolateral radiographic view with ~132° of extension, and **b)** sagittal computed reconstructed elbow tomographic image. A set of 13 or 14 points was marked at the central ridge of the ulnar trochlear notch, from the anconeal process to the base of the medial coronoid process, and on the adjacent humeral trochlear groove, respectively.

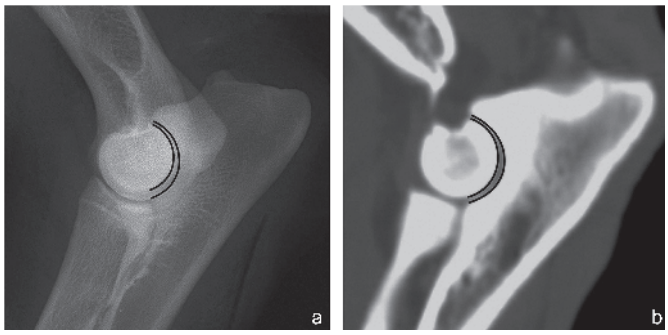

Figure 4 **a)** Mediolateral radiographic view with ~132° of extension, and **b)** sagittal computed reconstructed elbow tomographic image. The joint curves were traced by a curve-fitting process on the ulnar trochlear notch and on the humeral trochlear groove.

helical CT scanner[a], at 140 kV and 260 mAs, using a small field of view and a bone reconstruction filter. Each elbow was imaged separately with the lateral side down. Limbs were maintained in a neutral position with respect to pronation and supination, to limit artefactual alterations in congruity (21). Images were collected with a slice thickness of 1.3 mm and an overlapping increment of 0.6 mm.

Computer imaging analysis

All the radiographic views and CT images were recorded using digital support. Image analysis was performed on the UTN central ridge, from the anconeal process to the base of the medial coronoid process and on the HT sagittal groove in contact with the UTN on ~132° extension (▶Figure 1) (22). Elbow CT images were reconstructed using a bone window (window width 1500 and level 300 of Hounsfield units) with a DICOM viewer[b]. Multiplane reconstruction views were created to allow transverse, dorsal and sagittal images to be observed concurrently. Repeatable slice alignment of the UTN and HT, to be measured with the software on the CT images, was achieved by determining the central sagittal cross-section image (▶Figure 2). On the MLE view and on the reconstructed central sagittal elbow CT image, a set of 13 or 14 points was marked at subchondral level in the HT groove and UTN central ridge, respectively (▶Figure 3) (19, 20). Then, by curve fitting, the joint curves were traced using a software that had been developed (▶Figure 4) (19, 20). Three independent evaluation sessions of each curvature were performed by the same examiner (SAP). The sequence of radiographs and CT images was randomly chosen.

Anatomical preparation

The elbow joints were prepared using anatomical dissection. The humeroradioulnar joints were disarticulated using slow maceration and the articular surfaces of the UTN and HT were meticulously cleaned. The distribution of the cartilage covering was examined macroscopically and graded into categories by two examiners (MMG, SAP) in accordance with the classification system described by Probst and colleagues (15, 24):

- **Type one:** UTN surface totally covered with articular cartilage
- **Type two:** UTN articular cartilage covering with incomplete transverse separation
- **Type three:** UTN articular cartilage with complete transverse separation
- **Type four:** UTN articular cartilage covering reduced to the medial aspect with a cartilaginous islet area at the lateral coronoid process
- **Type five:** only the UTN medial component was covered with articular cartilage.

Statistical analysis

Data were assessed for normality using Shapiro-Wilk's test and descriptive analysis was performed. The intraclass correlation coefficient (ICC) and Bland-Altman analysis were used to evaluate intra-observer agreement in three independent measurement sessions and the agreement between measurements in the MLE views and CT images (25, 26). For statistical purposes, 20 curvature sequential radius points were used, which were selected by computer software at similar pre-established distances (~5%) from each other (25). An ICC value of one indicates perfect agreement and zero indicates no agreement (25). For the Bland-Altman method, if the 95% confidence interval (CI) of the mean difference (d) includes the zero, statistical agreement is indicated, and when the 95% lower and upper limits of agreement are small, then these two measurements can be considered equivalent (26).

Differences between UTN and HT measurements on the MLE view and CT images were analysed based on the similarity of the curvature radii behaviour observed along the two curves. The curvature radii extremes (proximal and distal), two intermediates peaks, and three intermediate minimum values were used to define

a Mx 8000 Philips Brilliance: Philips, Eindhoven, Netherlands
b Radiant, version 1.9.16: Medixant, Poznan, Poland

Table 1 Comparison between curvature radius measurements obtained at the mediolateral radiographic view and at the sagittal computed tomography image.

	Mediolateral radiographic view / CT measurements					
	ICC	ICC 95% CI	*d* ± SEM (mm)	*d* 95% CI (mm)	*d* ± SD (mm)	95% LA (mm)
UTN	0.85	0.82 to 0.88	-0.71 ± 0.13	-0.97 to -0.45	-0.71 ± 2.43	-5.48 to 4.06
HT	0.89	0.86 to 0.91	-1.04 ± 0.09	-1.21 to -0.87	-1.04 ± 1.64	-4.25 to 2.17

CI = confidence interval; CT = sagittal computed tomographic image; *d* = mean differences; HT = humeral trochlear groove; ICC = intraclass correlation coefficient; LA = limits of agreement; SD = standard deviation; SEM = standard error of the mean; UTN = ulnar trochlear notch.

the seven points of interest (P_1 to P_7). The anatomical position of these seven points in the radiographic and CT images were also calculated and represented in radiographic and CT images using computer software[c] to measure their anatomical localization in the joint.

All data were analysed using a standard computer software system[d] and $p < 0.05$ was considered significant.

Results

Comparison between radiographic and CT measurements

The intra-observer repeatability was statistically adequate in all three measurement sessions on each studied variable (UTN and HT in the MLE views and CT images) with all ICC lower limit 95% CI being greater than 0.75 and the *d* 95% CI include zero. The comparison between curvature radii in the MLE radiographic views and CT images showed an ICC of 0.85 with a 95% CI from 0.82 to 0.88 for the UTN; and an ICC of 0.89 with a 95% CI from 0.86 to 0.91 to the HT. The *d* between MLE and CT measurements were statically significant, the 95%CI of *d* did not include zero, being –0.71 mm (95% CI: –0.97 to –0.45) for UTN and –1.04 mm (95% CI: –1.21 to –0.87) for HT (▶Table 1).

Comparison between UTN and HT

In general the UTN and HT curvature radii had a similar typology (proximal and distal peaks, two intermediates peaks, and three intermediate minimum values) though the UTN curvature was bigger than the HT in both the MLE radiographic view and sagittal CT images (▶Figure 5). Some significant and non-significant differences were observed in the curvature radii of the UTN and the HT in these seven points of interest. The biggest differences were registered at the beginning of the curve (P_1) and on the second intermediate peak (P_5) (▶Table 2). The anatomical location of the seven points of interest at the UTN and HT on the radiographic and CT image are illustrated in Figure 6.

Articular cartilage covering

Four of 16 elbows were classified according to the articular cartilage covering as type one, showing complete surface of the UTN covered with cartilage; and 12 of 16 elbows were classified as type two, showing incomplete transverse separation in the UTN articular cartilage covering. None of the elbows were classified as type three, four or five.

Discussion

Accurate quantification of elbow joint congruity is important, both to guide potential clinical intervention and to advance our understanding on the aetiopathogenesis of developmental elbow disease (13, 18, 27). The absence of an appropriate imaging method for the accurate clinical diagnosis of humeroulnar incongruity makes this a more interesting challenge and the investigation of UTN and HT curvature radii can bring some important additional information on this issue.

We decided to assess the UTN and HT in contact at ~132° elbow angle, based on the elbow angle during the mid-stance phase of the canine gait cycle (13, 22, 23, 30). However, images using other joint angulations can also be used, since the anatomical UTN and HT areas for analysis are selected independently in images, based on ~132° elbow angulation and not by the visualized contact areas.

Our results showed good intra-observer agreement in repeated measurement sessions, with all ICC lower limits 95% CI

Table 2 Mean of the differences and 95% confidence interval observed between the ulnar trochlear notch and the humeral trochlear groove curvature radii at the seven points of interest (P_1 to P_7) selected in the mediolateral radiographic view and sagittal joint computed tomography reconstruction.

Selected points	Mean of the differences and 95% CI of UTN-HT curvature radii (mm)	
	Mediolateral radiographic view	Sagittal computed tomography image
P_1	6.25* (5.90 to 6.60)	2.94* (1.64 to 4.25)
P_2	1.03* (0.46 to 1.59)	1.94* (1.35 to 2.53)
P_3	1.41* (0.44 to 2.37)	0.30 (-1.19 to 1.78)
P_4	0.04 (-0.37 to 0.44)	-0.24 (-0.70 to 2.22)
P_5	1.77* (0.92 to 2.63)	1.94*(1.13 to 2.74)
P_6	0.86* (0.14 to 1.57)	0.93 (-0.02 to 1.88)
P_7	0.68 (-0.51 to 1.86)	0.83 (-1.51 to 3.16)

* $p < 0.05$; CI = confidence interval; UTN = ulnar trochlear notch; HT = humeral trochlear groove.

c Image Pro Plus, version 6: Media Cybernetics, Rockville, MD, USA

d SPSS Version 23: IBM Corp., Armonk, NY, USA

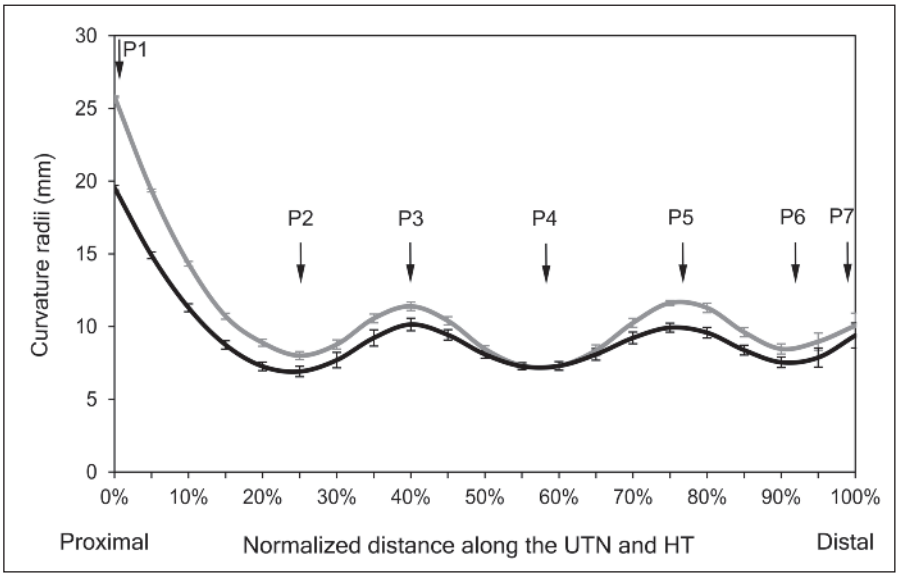

Figure 5 Relationship between the radii of curvature (mean ± standard error of the mean) found along the ulnar trochlear notch (UTN, grey) and the humeral trochlear groove (HT, black) on the mediolateral extended radiographic views. The seven points of interest (P_1 to P_7) used for statistical purposes were defined based on curvature typology as well as the maximum and minimum curvature radius values.

>0.75 and non-significant mean differences, so in future studies one measurement session could be enough. In fact, we found that marking the joint subchondral bone is fairly objective, resulting in quite a good level of similarity across different measuring sessions. We found a good correlation between the MLE radiographic views and sagittal CT images in the UTN and HT curvature radii, with a lower limit 95% CI >0.75 and similarity in the typology of both curves. However, in general, the CT curvature radii were slightly bigger (in UTN and HT) resulting in significant differences. This last fact was not expected and may be associated with some kind of radiographic or tomographic imaging artefact. We also found it easier to score bends using the CT rather than the MLE view, possibly due to the greater contrast observed between subchondral bone and joint space in the CT images and the absence of osseous structures superposition. However, *d* were very small (1 mm or less), and their 95%CI limits of agreement were small enough for us to consider them acceptable for clinical purposes, thus curvature radii measurements using radiographic and CT evaluation are identical and can be used interchangeably (25, 26).

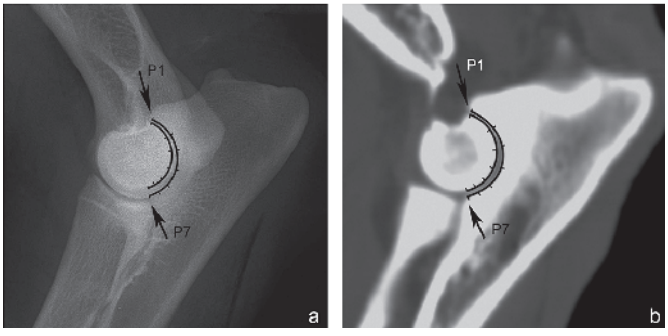

Figure 6 Illustration of the seven points of interest (P_1 to P_7) in the ulnar trochlear notch and in the humeral trochlear groove. **a)** Mediolateral extended radiographic view of the elbow. **b)** Sagittal computed tomography image of the elbow.

The curvature radius of a curve at a particular point can be defined as the radius of the approximate circle at that point (11). The radius dimension changes when we move along a curve, unless it is a circle. Larger curvature radii values correspond to a more open curve and smaller values correspond to a more enclosed curve. A bigger mean UTN radius curvature than HT was expected, as the UTN is the peripheral joint surface. The UTN and HT curvatures' different radii values along their extensions were also expected, due to their ellipsoid shapes (8). The definition of the points of interest (P_1 to P_7) based on the curvature radii behaviour (i.e. extremes and intermediates peaks of maximum and minimum curvature radius values) was not based on other studies and is only intended to be a way to objectively quantify the association of the UTN and HT radii curvature differences to the joint congruence. The curve areas with small UTN and HT radii differences (e.g. P_4), and others with larger differences (for, e.g., intermediate radii peaks, P_3 and P_5) that correspond to relatively flat areas can be fundamental to adequate joint load transmission. These findings may be also associated with some of this sample's characteristics, as the most representative (75%) of the joints had type two articular cartilage covering. The absence of cartilage recovery has been directly associated with a lower load bearing support in these regions (24). Previous biomechanical studies also report that some individuals had a bicentric load transmission through the humeroulnar joint at low loads with a lack of contact at the central UTN (7, 11). The areas of greater contact between joint surfaces in the elbow were established at the radial head, medial aspect of the distal UTN, and on the craniolateral surface of the proximal UTN (7, 28). Other studies also suggested a nearly bicentric, subchondral density associated with load transmission in the UTN (9, 11). Our curvature radii UTN and HT typology would allow a higher humeroulnar joint contact between P_1-P_3 and P_5-P_7 and lower between P_3-P_5.

Various authors have attempted to describe humeroulnar incongruity by measuring the joint spaces (6, 12). However, these parameters present some limi-

tations as joint spaces easily change depending on the limb positioning in radiographic and CT imaging (4-6, 29). The UTN and HT curvature radii measuring methodology presented in this report enables their evaluation separately and independent of joint angulation, which can be a very important factor in terms of clinical use (19, 20).

This was an *ex vivo* study that can be associated with several limitations, and the results should be interpreted with caution. First, radiography and CT are good diagnostic tools for assessing subchondral bone, however they cannot evaluate the integrity of the articular cartilage (4). Secondly, we only studied the UTN central ridge and the HT groove, not all joint structures. The step between the radius and ulna, which is also an important factor in elbow incongruity assessment, was not investigated in this study. Thus extrapolation of our results should be interpreted in this context.

Conclusions

To the best of the authors' knowledge, the present paper is the first report on humeroulnar curvature congruity assessment through curvature radius evaluation. Curvature radii measurements can be used interchangeably in the MLE radiographic views and sagittal CT images. The software and methodology proposed enabled accurate measurements of the humeroulnar curvature radii and may be useful in future clinical studies of elbow congruity for detection of early changes in elbow dysplasia. Further breed-specific studies would be necessary to assess the variation that may occur in the points of interest. Future comparative research between normal and dysplastic dogs would be useful to assess the early variation occurring at the points studied, and the role of incongruity in the development of elbow dysplasia.

Acknowledgements

The authors are grateful to Prof. Jorge Colaço for his statistical assistance. The authors would like to acknowledge Mr. João Gonçalves and Mr. Filipe Fontinha for assistance in the anatomic bone preparation. Armando Fernandes is thankful to FCT – Portuguese Foundation for Science and Technology for his post-doctoral research grant number SFRH/BPD/108060/2015.

Financial Support

This work is supported by: European Investment Funds by FEDER/COMPETE/POCI– Operational Competitiveness and Internationalization Program, under Project POCI-01–0145-FEDER-006958 and National Funds by FCT – Portuguese Foundation for Science and Technology, under the project UID/AGR/04033.

Conflict of interest

The authors declare no conflict of interest related to this report.

References

1. Lau SF, Hazewinkel HAW, Voorhout G. Radiographic and computed tomographic assessment of the development of the antebrachia and elbow joints in Labrador Retrievers with and without medial coronoid disease. Vet Comp Orthop Traumatol 2015; 28: 186–192.
2. Coppieters E, Gielen I, Verhoeven G, et al. Erosion of the medial compartment of the canine elbow: occurrence, diagnosis and currently available treatment options. Vet Comp Orthop Traumatol 2015; 28: 9–18.
3. Coopman F, Broeckx B, Verelst E, et al. Combined prevalence of inherited skeletal disorders in dog breeds in Belgium. Vet Comp Orthop Traumatol 2014; 27: 395–397.
4. Skinner OT, Warren-Smith CMR, Burton NJ, et al. Computed tomographic evaluation of elbow congruity during arthroscopy in a canine cadaveric model. Vet Comp Orthop Traumatol 2015; 28: 19–24.
5. Samoy YCA, De Bakker E, Van Vynckt D, et al. Arthroscopic treatment of fragmented coronoid process with severe elbow incongruity long-term follow-up in eight Bernese Mountain Dogs. Vet Comp Orthop Traumatol 2013; 26: 27–33
6. Burton NJ, Warren-Smith CMR, Roper DP, et al. CT assessment of the influence of dynamic loading on physiological incongruency of the canine elbow. J Small Anim Pract 2013; 54: 291–298.
7. Preston CA, Schulz KS, Kass PH. In vitro determination of contact areas in the normal elbow joint of dogs. Am J Vet Res 2000; 61: 1315–1321.
8. Wind AP. Elbow incongruity and developmental elbow diseases in the dog: part I. J Am Anim Hosp Ass 1986; 22: 711–724.
9. Dickomeit MJ, Böttcher P, Hecht S, et al. Topographic and age-dependent distribution of subchondral bone density in the elbow joints of clinically normal dogs. Am J Vet Res 2011; 72: 491–499.
10. De Rycke LM, Gielen IM, van Bree H, et al. Computed tomography of the elbow joint in clinically normal dogs. Am J Vet Res 2002; 63: 1400-1407.
11. Eckstein F, Merz B, Schmid P, et al. The influence of geometry on the stress distribution in joints, a finite element analysis. Anat Embryol 1994; 189: 545–552.
12. Samoy Y, Gielen I, Saunders J, et al. Sensitivity and specificity of radiography for detection of elbow incongruity in clinical patients. Vet Radiol Ultrasound 2011; 53: 236-244.
13. Proks P, Necas A, Stehlik L, et al. Quantification of humeroulnar incongruity in Labrador retrievers with and without medial coronoid disease. Vet Surg 2011; 40: 981–986.
14. Stein S, Schmoekel HG, Waibl H, et al. Computerized measurements of radiographic anatomical parameters of the elbow joint in Bernese mountain dogs. Vet Comp Orthop Traumatol 2012; 25: 250–261.
15. Janach KJ, Breit SM, Künzel WWF. Assessment of the geometry of the cubital (elbow) joint of dogs by the use of magnetic resonance imaging. Am J Vet Res 2006; 67: 211–217.
16. Wolschrijn CF, Kik MJL, Weijs WA. Cartilage-free areas in the elbow joint of young golden retrievers. Anat Rec A Discov Mol Cell Evol Biol 2003; 275: 990–996.
17. Mason DR, Schulz KS, Fujita Y, et al. In vitro force mapping of normal canine humeroradial and humeroulnar joints. Am J Vet Res 2005; 66: 132–135.
18. Eljack H, Werner H, Böttcher P. Sensitivity and specificity of 3D models of the radioulnar joint cup in combination with a sphere fitted to the ulnar trochlear notch for estimation of radioulnar incongruence in vitro. Vet Surg 2013; 42: 365–370.
19. Alves-Pimenta S, Ginja MM, Colaço J, et al. Curvature radius measurements from the ulnar trochlear notch in large dogs. Anat Rec 2015; 298: 1748–1753.
20. Alves-Pimenta S, Ginja MM, Fernandes AM, et al. Curvature radius measurements from the humeral trochlea in large dogs. Anat Rec 2016; 299: 1012–1014.
21. House MR, Marino DJ, Lesser ML. Effect of limb position on elbow congruity with CT evaluation. Vet Surg 2009; 38: 154–160.
22. DeCamp CE, Soutas-Little RW, Hauptman J, et al. Kinematic gait analysis of the trot in healthy greyhounds. Am J Vet Res 1993; 54: 627–634.
23. Collins KE, Cross AR, Lewis DD, et al. Comparison of the radius of curvature of the ulnar trochlear notch of Rottweilers and Greyhounds. Am J Vet Res 2001; 62: 968–973.
24. Probst A, Modler F, Künzel W, et al. Demonstration of the articular cartilage of the canine ulnar trochlear notch using high-field magnetic resonance imaging. Vet J 2008; 177: 63–70.
25. Lee J, Koh D, Ong CN. Statistical evaluations of agreement between two methods for measuring a quantitative variable. Comput Biol Med 1989; 19: 61–70.
26. Bland JM, Altman DG. Statistical methods for assessing agreement between two methods of clinical measurement. Lancet 1986; 1: 307–310.

27. Samoy Y, Gielen I, Van Caelenberg A, et al. Computed tomography findings in 32 joints affected with severe elbow incongruity and fragmented medial coronoid process. Vet Surg 2012; 41: 486–494.
28. Cuddy LC, Lewis DD, Kim SE, et al. Contact mechanics and three dimensional alignment of normal dog elbows. Vet Surg 2012; 41: 818-828.
29. Goodrich ZJ, Norby B, Eichelberger BM, et al. Thoracic limb alignment in healthy Labrador Retrievers: Evaluation of standing versus recumbent frontal plane radiography. Vet Surg 2014; 43: 791–803.
30. Lorenz ND, Channon S, Pettitt R, et al. Ex vivo kinematic studies of a canine unlinked semi-constrained hybrid total elbow arthroplasty system. Vet Comp Orthop Traumatol 2015; 28: 39–47.